remote sensing

MDPI

Article

The Effect of a Parcel-Aggregated Cropping Structure Mapping Method in Irrigation-Water Estimation in Arid Regions—A Case Study of the Weigan River Basin in Xinjiang

Haoyu Wang [1,2,3,4,5], Linze Bai [6], Chunxia Wei [7], Junli Li [1], Shuo Li [2,8], Chenghu Zhou [2,9], Philippe De Maeyer [3,4,5], Wenqi Kou [2,8], Chi Zhang [2,8], Zhanfeng Shen [2,8,*] and Tim Van de Voorde [3,4,5]

1 National Key Laboratory of Ecological Security and Sustainable Development in Arid Region, Xinjiang Institute of Ecology and Geography, Chinese Academy of Sciences, Urumqi 830011, China; haoyu.wang@ugent.be (H.W.); lijl@ms.xjb.ac.cn (J.L.)
2 University of Chinese Academy of Sciences, Beijing 100049, China; lishuo191@mails.ucas.ac.cn (S.L.); zhouch@lreis.ac.cn (C.Z.); kouwenqi22@mails.ucas.ac.cn (W.K.); zhangchi233@mails.ucas.ac.cn (C.Z.)
3 Department of Geography, Ghent University, 9000 Ghent, Belgium; philippe.demaeyer@ugent.be (P.D.M.); tim.vandevoorde@ugent.be (T.V.d.V.)
4 Sino-Belgian Joint Laboratory of Geo-Information, 9000 Ghent, Belgium
5 Sino-Belgian Joint Laboratory of Geo-Information, Urumqi 830011, China
6 School of Earth Sciences, Zhejiang University, 866 Yuhangtang Rd., Hangzhou 310058, China; bolizer@zju.edu.cn
7 Xinjiang Tarim Populus Euphratica National Nature Reserve Administration, Korla 841000, China
8 National Engineering Research Center for Geomatics, Aerospace Information Research Institute, Chinese Academy of Sciences, Beijing 100101, China
9 State Key Laboratory of Resources and Environmental Information System, Institute of Geographic Sciences and Natural Resources Research, Chinese Academy of Sciences, Beijing 100101, China
* Correspondence: shenzf@radi.ac.cn; Tel.: +86-186-1114-9939

check for updates

Citation: Wang, H.; Bai, L.; Wei, C.; Li, J.; Li, S.; Zhou, C.; De Maeyer, P.; Kou, W.; Zhang, C.; Shen, Z.; et al. The Effect of a Parcel-Aggregated Cropping Structure Mapping Method in Irrigation-Water Estimation in Arid Regions—A Case Study of the Weigan River Basin in Xinjiang. *Remote Sens.* **2024**, *16*, 3941. https://doi.org/10.3390/rs16213941

Academic Editor: Konstantinos X. Soulis

Received: 26 August 2024
Revised: 18 October 2024
Accepted: 22 October 2024
Published: 23 October 2024

Copyright: © 2024 by the authors. Licensee MDPI, Basel, Switzerland. This article is an open access article distributed under the terms and conditions of the Creative Commons Attribution (CC BY) license (https://creativecommons.org/licenses/by/4.0/).

Abstract: Effective management of agricultural water resources in arid regions relies on precise estimation of irrigation-water demand. Most previous studies have adopted pixel-level mapping methods to estimate irrigation-water demand, often leading to inaccuracies when applied in arid areas where land salinization is severe and where poorly growing crops cause the growing area to be smaller than the sown area. To address this issue and improve the accuracy of irrigation-water demand estimation, this study utilizes parcel-aggregated cropping structure mapping. We conducted a case study in the Weigan River Basin, Xinjiang, China. Deep learning techniques, the Richer Convolutional Features model, and the bilayer Long Short-Term Memory model were applied to extract parcel-aggregated cropping structures. By analyzing the cropping patterns, we estimated the irrigation-water demand and calculated the supply using statistical data and the water balance approach. The results indicated that in 2020, the cultivated area in the Weigan River Basin was 5.29×10^5 hectares, distributed over 853,404 parcels with an average size of 6202 m^2. Based on the parcel-aggregated cropping structure, the estimated irrigation-water demand ranges from 25.1×10^8 m^3 to 30.0×10^8 m^3, representing a 5.57% increase compared to the pixel-level estimates. This increase highlights the effectiveness of the parcel-aggregated cropping structure in capturing the actual irrigation-water requirements, particularly in areas with severe soil salinization and patchy crop growth. The supply was calculated at 24.4×10^8 m^3 according to the water balance approach, resulting in a minimal water deficit of 0.64×10^8 m^3, underscoring the challenges in managing agricultural water resources in arid regions. Overall, the use of parcel-aggregated cropping structure mapping addresses the issue of irrigation-water demand underestimation associated with pixel-level mapping in arid regions. This study provides a methodological framework for efficient agricultural water resource management and sustainable development in arid regions.

Keywords: parcel; cropping structure; irrigation estimation; water balance

1. Introduction

Agriculture is the foundation for socio-economic development and is the comprehensive result of resource utilization and human transformation [1–3]. Efficient agricultural water management is unachievable in arid regions with limited water resources. In recent years, initiatives such as permanent basic farmland protection and national standard farmland renovation in China have decreased farmland areas and improved farmland structures. However, considering the actual situation where farmland conditions remain variable, the application of water-saving irrigation techniques and water resource management [4,5] necessitates the rapid and precise updating of crop structures.

Crop structure defines crop distribution and plays a critical role in various agricultural activities, including crop health diagnosis, agricultural disaster evaluation, and yield prediction [6]. Additionally, mapping accurate crop structures is essential for estimating agricultural water in water-scarce regions [7], as irrigation water is often allocated based on the type and water requirements of planted crops. The traditional method of obtaining cropping structure mainly relies on comprehensive data provided by yearbooks or administrative units, which suffer from poor timeliness and low spatial resolution, making it difficult to meet the requirement of the irrigation-water demand estimation at a refined spatial scale.

Compared with traditional methods, remote sensing technologies can quickly and accurately acquire surface crop information at large scales and are identified as efficient measures to manage irrigation water [8]. For example, Sobhan et al. [9] identified changes in cropping patterns in an irrigation system and estimated irrigation-water demand by integrating optical and microwave remote sensing data; Han et al. [10] used remote sensing technology to analyze the effects of cropping restructuring on the water-use efficiency of irrigation districts in the Heihe River Basin; and Ma et al. [11] evaluated crop water productivity and optimized the planting structure in Qira Oasis using a dynamic Bayesian network. In addition, there are a large number of studies that quantify evapotranspiration and biomass production through remote sensing data to estimate regional irrigation-water demand [12–15].

However, these studies are inconsistent with the actual situation when applied to estimate irrigation-water demand in arid zones. The reason is that most of the studies used a mapping method at the pixel level, while the irrigation plan is usually made based on the area of agricultural parcels. Particularly in the arid region of Xinjiang, where land salinization is a serious issue, there are poorly growing crops in some large fields, resulting in the growing area being smaller than the sown area. Pixel-level mapping often ignores these poorly growing areas, leading to underestimation of irrigation-water demand. Therefore, a parcel-aggregated planting structure is more suitable to estimate irrigation-water demand.

As the application of deep learning techniques [16–18] to extract complex spatial information matures, more and more studies have used them for mapping parcel-aggregated planting structures [19–22]. However, no study has yet applied the parcel-aggregated cropping structure to irrigation-water demand estimation in arid areas. To evaluate the impact of parcel-aggregated cropping structure mapping methods on irrigation-water estimation in arid regions, this paper proposes a deep learning-based framework to extract parcel-aggregated cropping structures. Using this framework, we obtained the parcel-aggregated cropping structure of the Weigan River Basin of Xinjiang, China, and subsequently estimated the irrigation-water demand based on it. Afterward, the irrigation-water demand calculated by the parcel-aggregated cropping structure was compared with that obtained by the pixel-level method. Finally, the irrigation-water supply was calculated using a water balance approach, aiming to provide a scientific basis for further optimizing agricultural water use. The subsequent sections of this paper are organized as follows: Section 2 describes the study area and data used. Section 3 details the methodology, including the parcel-aggregated cropping structure mapping and irrigation supply and demand calcu-

lations. Sections 4 and 5 present the results, analysis, and discussion. Finally, the main conclusions are drawn in Section 6.

2. Study Area and Data Preparation

The Weigan River Basin (Figure 1) is situated in the northern section of the Tarim Basin in Xinjiang, China, spanning from 40°55′ to 41°20′N and 82°30′ to 83°30′E, with elevations ranging from 900 to 2500 m. The basin is characterized by a typical pre-mountain impact fan-shaped plain and includes critical urban areas such as Kuche, Shaya, and Xinhe. The catchment area of the basin covers 2.76 × 10^4 km^2. The region has extreme aridity, frequent windy conditions, and significant temperature fluctuations between day and night, indicative of a typical continental warm temperate climate. The annual precipitation, mainly from April to July, varies between 51 and 67 mm, while the average annual evaporation varies between 2000 and 2010 mm [23]. The primary crops grown in the region include cotton, corn, peppers, and tomatoes, with cotton being the most widely cultivated, covering 70% of the total arable land [24]. The main rivers in the basin are the Weigan River, the Kuche River, the Indaria River, the mainstream of the Tarim River, and some small tributaries. According to the river trend, the Heizi, Langan, and Alaer reservoirs are selected as the intakes and Yingbazha reservoir as the outlet, forming a relatively closed water balance cycle system.

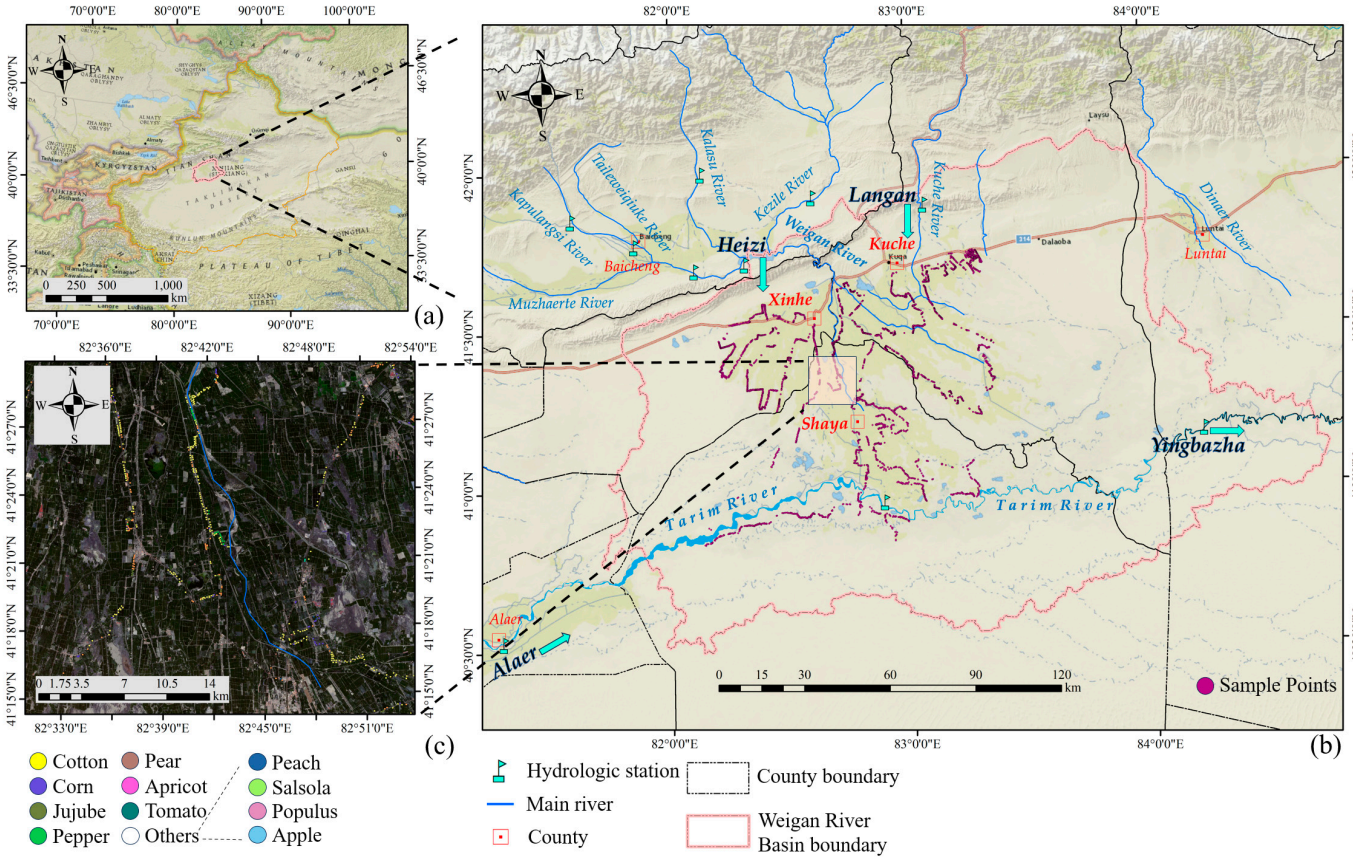

Figure 1. Location of the study area. (**a**) The study area is located in the northern section of the Tarim Basin in Xinjiang, China; (**b**) a detailed map of the study area, including rivers, hydrological stations, sampling points, and their types; (**c**) the zoomed-in Google Earth imagery of the study area and field sampling points.

Our research used Google Earth true-color imagery from 2020 with a 1 m spatial resolution to extract parcels. For the extraction of the cropping structure, we used Sentinel-2 optical remote sensing data with a 10 m spatial resolution, as shown in Table 1. We

preprocessed these Sentinel-2 images using the European Space Agency's SNAP software with version 10.0.0 and implemented a cloud removal step to eliminate interference from cloud cover. Following the preprocessing, we merged and cropped the data using ENVI software with version 5.3.1. Meteorological and hydrological data for the study were obtained from various sources such as scientific research stations, statistical yearbooks, bulletins, etc. Further details regarding the data sources will be provided in subsequent sections. Field surveys were conducted in the summer of 2020, collecting 2418 valid farmland sample points after eliminating duplicate and offset sample points. These sample points were utilized for crop identification and labeling purposes. The other data used in this study are shown in Table 2.

Table 1. The Sentinel-2 images used in this study.

Date	Day of Year	Date	Day of Year	Date	Day of Year
6 January 2020	6	5 May 2020	126	2 September 2020	246
21 January 2020	21	20 May 2020	141	17 September 2020	261
5 February 2020	36	4 June 2020	156	2 October 2020	276
20 February 2020	51	19 June 2020	171	17 October 2020	291
6 March 2020	66	4 July 2020	186	1 November 2020	306
21 March 2020	81	19 July 2020	201	16 November 2020	321
5 April 2020	96	3 August 2020	216	1 December 2020	336

Table 2. Description of the data used in this study.

Category	Subcategory	Period	Description
Remote sensing imagery	Google Earth imagery	2020	1. True-color with 1 m spatial resolution 2. Used for parcel extraction
	Sentinel-2 imagery		1. Four bands (B, G, R, IR) with 10 m spatial resolution 2. Used for parcel classification
Parcel-level cultivated land sample point	–	2020	Constructing training, validation, and testing set
Agricultural irrigation-water quotas for 8 crops	Kuche Shaya Xinhe Yuli Luntai	2014	1. Data derived from Xinjiang Uygur Autonomous Region Agricultural Irrigation-water Quota Indicators 2. Used for calculating irrigation-water requirements for crops
Hydrological data	Surface runoff (Heizi, Langan, Aral, Yingbazha) Quantity of underground water resources	2020	1. Data derived from Water Resources Bulletin, Xinjiang Statistical Yearbook and Aksu Region Statistical Yearbook 2. Used for water consumption calculations
Water consumption in each county (Kuche, Shaya, Xinhe, Yuli, Luntai)	Industrial Livestock Daily life Vegetation		

3. Methods

3.1. Overview of the Method

This study proposes a strategy for remote sensing-based analysis of irrigation supply and demand in arid regions. Figure 2 shows the flowchart of the method, which comprises two parts:

1. Parcel-Aggregated Cropping Structure Mapping: The Richer Convolutional Features (RCF) model was used to extract candidate parcels from a single, very-high-spatial-resolution (VHR) image. Candidate parcels were then manually corrected to produce the final parcels, avoiding the accumulation of errors. Consequently, the spatially averaged NDVI temporal profiles of the sample parcels were constructed based on time-series Sentinel-2 images. Finally, the LSTM model was used to infer the crop types of all parcels, establishing the parcel-aggregated cropping structure of the study area.
2. Irrigation Analysis: The precise irrigation-water demand in the study area was obtained using the parcel-aggregated cropping structure, along with the irrigation efficiency of the study area and the water consumption of each crop from statistical data. The irrigation-water supply was calculated using statistics and a water balance approach. Conclusions and optimization recommendations were given by analyzing the relationship between irrigation supply and demand.

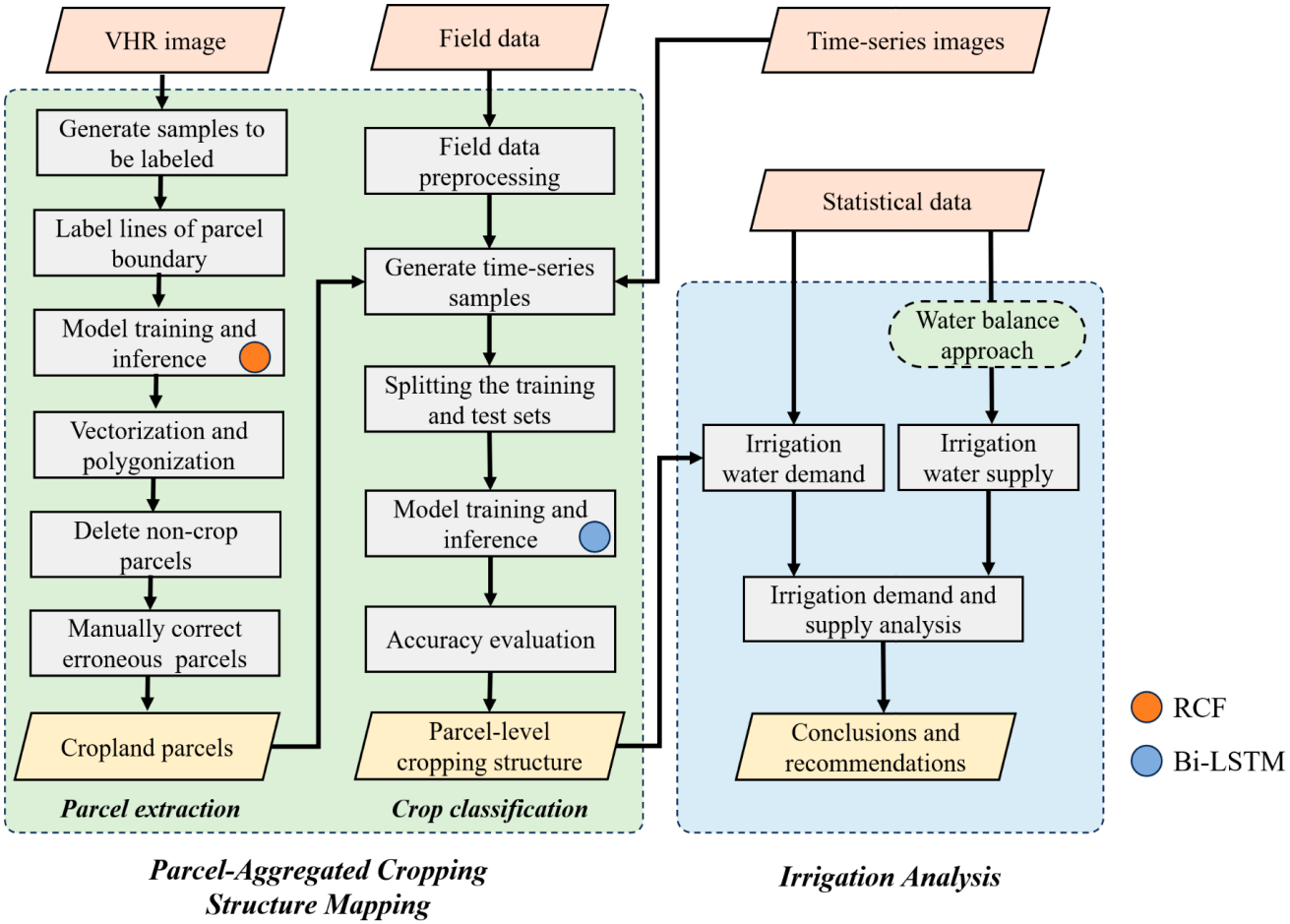

Figure 2. Flowchart of the proposed three-step method used to analyze irrigation-water supply and demand. Step 1 is parcel-aggregated cropping structure mapping; step 2 is irrigation analysis.

3.2. Parcel-Aggregated Cropping Structure Mapping

3.2.1. Parcel Extraction

The distinct edges of cultivated land in VHR images make it feasible to utilize deep-learning techniques for parcel extraction. This study uses the RCF model for parcel extraction [17] as follows:

(1) A uniformly distributed sample set of cultivated land parcels was created, which consists of 57 images, each measuring 1000 × 1000 pixels.

(2) The sample set was preprocessed and enhanced, including random cropping, rotation, and slight color transformation with a random value between 0 and 0.03. The sample set was expanded to 1386 images through this process.
(3) An RCF model was trained based on the enhanced sample set. The framework for model training was developed based on PyTorch. The ADAM [25] optimizer was utilized with an exponential learning rate decay. The loss function, FocalLoss [26], was used to penalize discrepancies between actual labels and model predictions, which enables more effective handling of class imbalance problems in edge extraction. Hyperparameters were set as follows: the initial learning rate was 0.01, the batch size was 8, and the number of training epochs was 300.
(4) The trained model was applied to infer the cropland parcels from the entire image of the study area. The inference applied 10% overlap patches that matched the size of the training image and finally obtained the raster parcels.
(5) The raster farmland parcels were vectorized and polygonized to obtain preliminary parcels.
(6) The preliminary vector farmland parcels were verified and edited manually to obtain the final vector parcels.

3.2.2. Crop Classification

Different crops exhibit distinct phenological information (Table 3), creating unique temporal image features. The NDVI temporal curve effectively represents these temporal features and is widely used in crop-type identification [19]. The NDVI was calculated as follows:

$$NDVI = \frac{\rho_{NIR} - \rho_{Red}}{\rho_{NIR} + \rho_{Red}} \quad (1)$$

where ρ_{NIR} is the reflectance value of the near-infrared band, and ρ_{Red} is the reflectance value of the red band.

Table 3. The phenology of the main crops in the Weigan River Basin. The distinctive phenological characteristics of crops are key to distinguishing their types.

Month	**Mar.**			**Apr.**			**May**			**Jun.**			**Jul.**			**Aug.**			**Sep.**			**Oct.**		
Period	B	M	E	B	M	E	B	M	E	B	M	E	B	M	E	B	M	E	B	M	E	B	M	E
Cotton					Sowing		Seedling emergence					Bud stage	Flowering			Boll opening						Harvest		
Corn					Sowing		Seedling emergence			Jointing			Heading				Grain filling		Harvest					
Jujube						Germination		Leaf expansion		Flowering			Growth						Harvest					
Pepper				Sowing			Seedling emergence			Transplanting			Growth			Flowering			Fruiting			Harvest		
Pear			Regreening				Leaf expansion			Growth			Harvest											
Apricot	Germination			Flowering			Leaf expansion			Fruiting			Harvest			Leaf fall								
Tomato				Sowing			Flowering			Growth			Harvest											

Time-series curves of the main crops (cotton, corn, jujube, chili, pear, apricot, and tomato) in the study area, along with the average temporal curve of other crops, as shown in Figure 3. For better characterization, we used the Savitzky–Golay convolution smoothing algorithm [25] (with a filtering window width set to 5 and a smoothing polynomial order set to 2) to smooth the curves. The smoothed curves facilitate a more evident observation of the crop's peak and valley features at different time intervals, corresponding to Table 3.

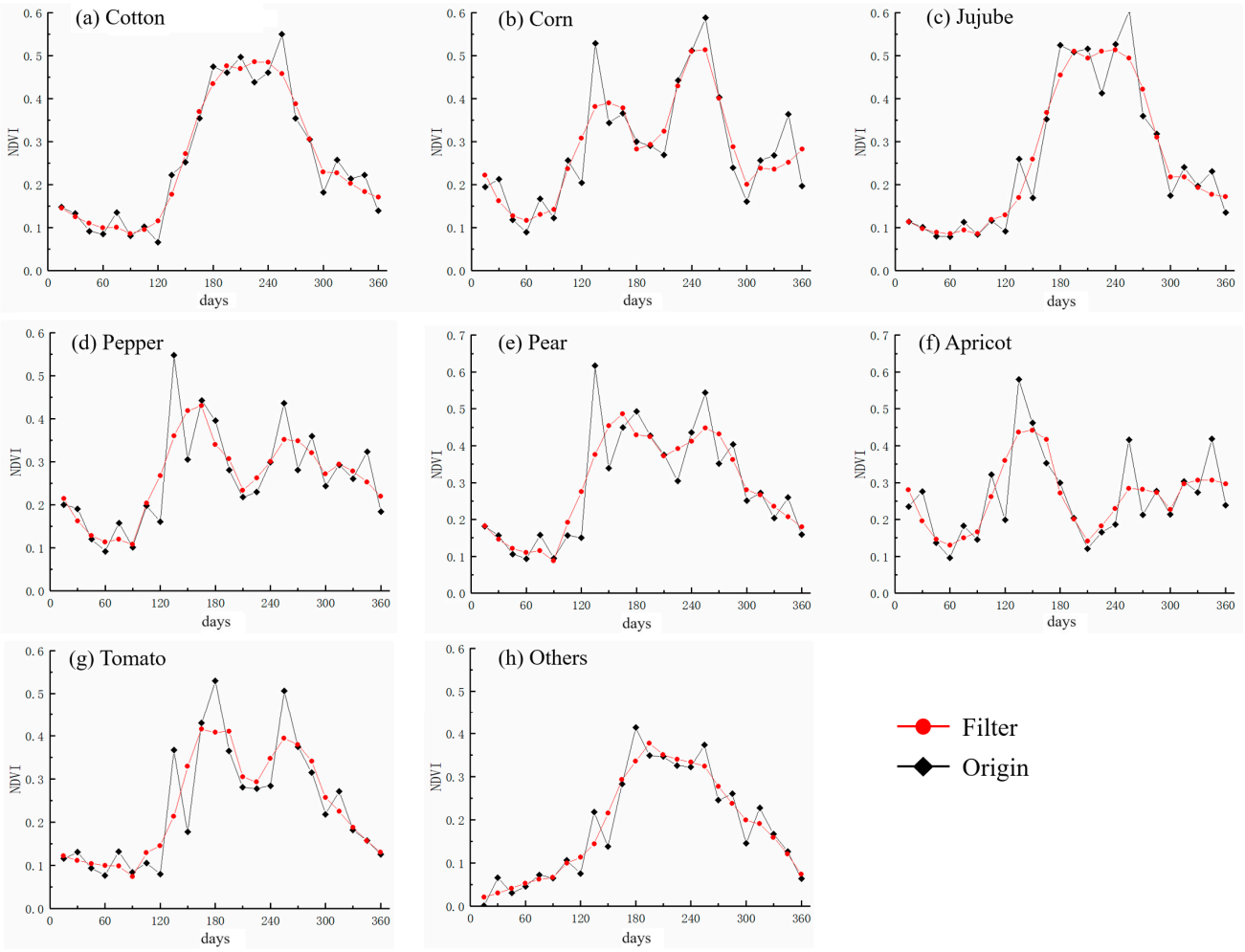

Figure 3. Growth curves of different crops. The black line denotes the original curve, while the red line illustrates the smoothed outcome obtained by applying the Savitzky–Golay convolution smoothing algorithm to the original curve. (**a**–**g**) corresponds to seven major crops in the study area, and (**h**) is the average curve for the other crops.

The LSTM model has been used in time-series analysis for remote sensing applications [26–28] and is thus used to classify crops based on NDVI curves. The specific process is outlined below:

(1) The crop categories were labeled for 3770 randomly selected parcels based on time-series imagery and sampling points. Then, we divided these parcels into training, validation, and test sets in the ratio of 6:1:3.
(2) The NDVI temporal curves were calculated, and then the Savitzky–Golay convolution smoothing algorithm was applied to each parcel's original curve.
(3) Model training was conducted on the training set using the designed bilayer LSTM model (Bi-LSTM) with 18 hidden cells. The framework for model training was developed based on PyTorch. The optimizer used was ADAM, and the loss function was the cross-entropy loss function [29]. The hyperparameters were set as follows: the initial learning rate was 0.001, the batch size was 16, and the number of training epochs was 100. The accuracy metrics were calculated on the test set.
(4) The trained Bi-LSTM model was used for inference to determine the crop categories of all parcels. Finally, the accuracy evaluation was performed.

The accuracy metrics comprised F1 score (F1), average F1 score (average F1), and weighted F1 score (weighted F1), calculated as follows:

$$P = TP/(TP + FP) \tag{2}$$

$$R = TP/(TP + FN) \tag{3}$$

$$F1 = 2{\cdot}(P \times R)/(P + R) \tag{4}$$

$$F1_{Average} = \frac{1}{N}\sum_{i=1}^{N} F1_i \tag{5}$$

$$F1_{Weighted} = \sum_{i=1}^{N} \omega_i F1_i \tag{6}$$

where TP is true positive and represents correctly classified parcels; FP is false positive and represents incorrectly classified parcels; and FN is false negative, representing incorrectly classified parcels as unfavorable. $F1_{Average}$ is calculated by taking the average of the $F1$ scores of all classes, treating each class equally regardless of its number of samples. And $F1_{Weighted}$ is calculated by taking the mean of the $F1$ scores of all classes, weighted by the number of samples in each class. N is the number of classes, and ω_i is the proportion of samples of class i in the dataset.

3.3. Irrigation Estimation

The irrigation demand is obtained by multiplying the irrigated area with the corresponding integrated irrigation quota:

$$Q = \sum_{i=1}^{n} Q_i = \sum_{i=1}^{n} m_i \times A_i \tag{7}$$

where Q is the irrigation-water demand of the study area (m^3); Q_i is the irrigation-water demand of the crop i (m^3); A_i is the planting area of the crop i. m_i is the irrigation quota for the crop i (m^3/a), which is calculated as follows:

$$mi = \sum_{t=1}^{n} \frac{m_t}{\eta_t} \times p_t \tag{8}$$

where m_t is the net irrigation-water quota for the crop, referring to the net irrigation-water consumption per unit area (m^3/a) throughout the crop growth cycle, including the preparation period; η_t is the coefficient of water resource utilization for the different irrigation methods; and p_t is the percentage of the crop planting area using this irrigation method relative to the total crop planting area.

The irrigation supply can be estimated based on a water balance approach [30]:

$$W_u + W_r + W_p = W_e + W_l + W_s + W_i + W_f \tag{9}$$

where W_u is the unduplicated groundwater resources for the year; W_r is the surface runoff for the year; W_p is the available precipitation for the year; W_s is the livestock water consumption for the year; W_l is the domestic water consumption for the year; W_e is the ecological water consumption for the year; W_i is the industrial water consumption for the year; and W_f is the irrigation-water supply for each year.

4. Results and Analysis

4.1. Cropping Structure Mapping Result

The parcel-aggregated cropping structure in the study area is illustrated in Figure 4. The cropland is mainly distributed along the riverbanks. In the upstream and midstream regions, smallholder farming prevails, featuring smaller and more diverse plots of land. In contrast, the downstream areas and locations farther from the river are characterized by large, contiguous fields primarily dedicated to cotton cultivation. Overall, the parcels in the study area, especially the large, rectangular fields, exhibit a regular shape. The ex-

tracted parcels are uniform and accurately depict the smallest operational unit of farmland management. Compared to pixel-level crop classification, parcel-level crop classification results are more regularized and free from salt-and-pepper noise, making them suitable for subsequent irrigation-water demand estimation.

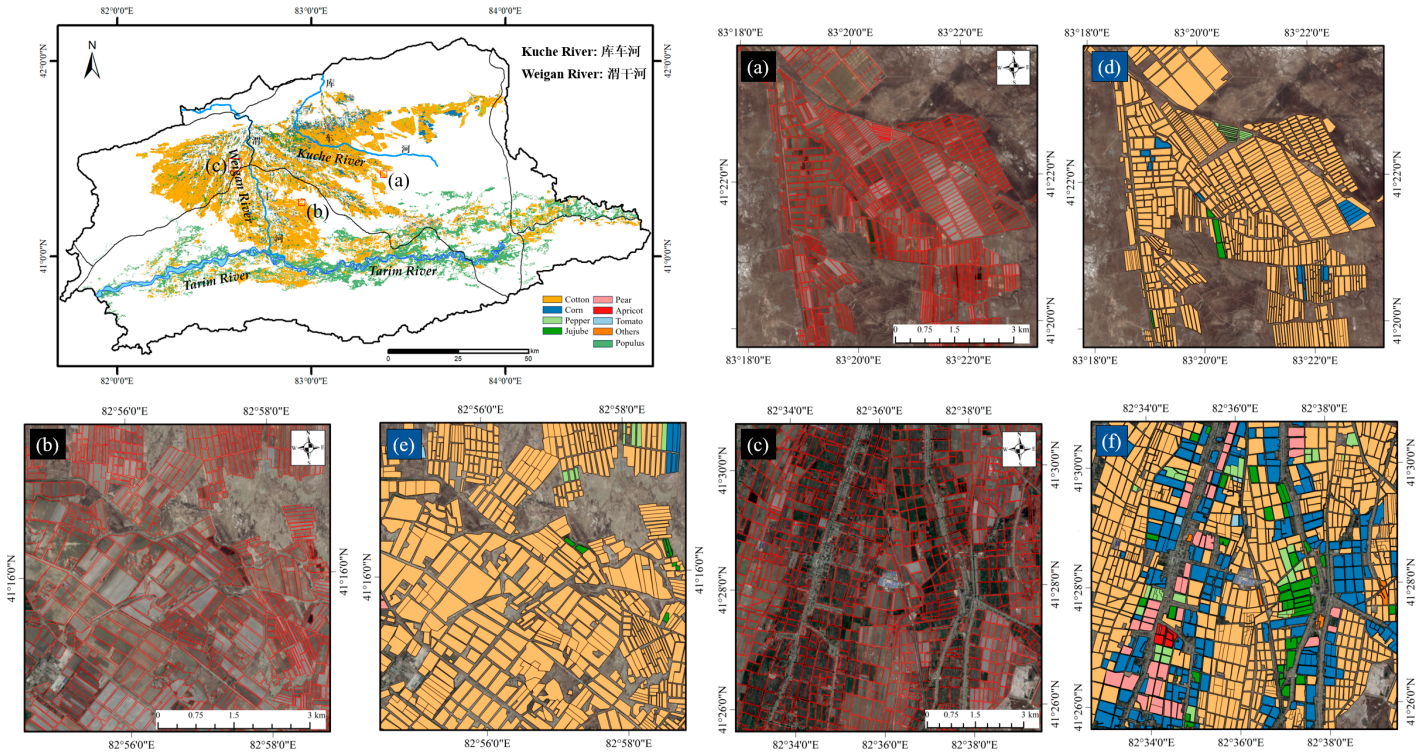

Figure 4. Illustration of parcel-aggregated cropping structure mapping result: (**a**–**c**) zoom-in parcel extraction result; (**d**–**f**) zoom-in crop classification results corresponding to (**a**–**c**).

We compared the classification results of multiple time-series models. The models included in the comparison are Transformer [31], Reformer [32], FEDformer [33], Crossformer [34], Dlinear [35], LightTS [36], PatchTST [37], FiLM [38], and TimesNet [39]. The experiment used the same dataset in Section 3.2.2 and retained the model with the highest accuracy after five independent training sessions. The hyperparameter configuration for Bi-LSTM can be found in Section 3.2.2. The remaining models were all set with an initial learning rate of 0.001, a maximum of 100 epochs, a batch_size of 16, a loss function of CrossEntropyLoss, and the optimizer ADAM. The accuracy evaluation metric displayed is the F1 score for each crop category. Additionally, the average F1 and weighted F1 were calculated. The weights for the weighted F1 are as follows: 0.8 for cotton, 0.05 for corn, and 0025 for all other crops.

The accuracy evaluation result is shown in Table 4, and the Figure 5 visualizes the extraction results of different models. Almost all models can accurately distinguish the category with the largest number of samples—cotton—while the accuracy for other categories with fewer samples decreases to varying extents. Transformer and its variants, such as Reformer, FEDformer, Crossformer, PatchTST, and TimesNet, performed well. Among these models, Reformer achieved the highest average F1 score of 0.849, and the weighted F1 scores of all models were generally above 0.9, with the lowest being 0.884 (Crossformer). In contrast, models like LightTS, DLinear, and FiLM exhibited significantly lower accuracy, with average F1 scores below 0.6. LightTS employs a lightweight MLP structure for sampling; DLinear decomposes time-series data into trend and residual components and models them using two separate single-layer linear networks; FiLM retains high-dimensional representations of Legendre projections to preserve all essential details

from historical data. The poor performance of these three models can be attributed to their lightweight designs, as the number of parameters in LightTS and DLinear is inherently insufficient to capture subtle temporal characteristics among different crop types. FiLM, on the other hand, tends to overlook peaks in time-series data, which are critical for identifying crop growth patterns. In comparison, models based on Transformer and LSTM architectures are more prone to overfitting these peaks in temporal data, allowing them to differentiate crop categories more precisely. It is worth noting that while the average F1 score better represents a model's classification performance under imbalanced sample conditions, for irrigation-water estimation, classification accuracy in categories with larger sample sizes is more important. Therefore, we selected Bi-LSTM, which achieved the highest weighted F1 score, as the final crop classification model.

Table 4. Accuracy evaluation results of crop classification based on different time-series models. The evaluation index of classification accuracy for each crop type is the F1 score. The highest value for each crop classification is emphasized in bold.

Model	Cotton	Corn	Jujube	Pepper	Pear	Apricot	Tomato	Others	Average F1	Weighted F1
Transformer	0.942	0.796	0.814	0.777	0.847	0.909	0.627	0.843	0.819	0.914
Reformer	0.947	0.81	0.724	0.683	0.884	**0.919**	**0.889**	0.934	**0.849**	0.924
FEDformer	0.940	0.775	0.754	0.489	0.881	0.821	0.712	**0.952**	0.791	0.906
Crossformer	0.914	0.708	0.717	0.755	0.696	0.776	0.844	0.883	0.787	0.884
DLinear	0.897	0.626	0.338	0.252	0.716	0.756	0.487	0.395	0.558	0.822
LightTS	0.909	0.690	0.491	0.363	0.769	0.697	0.504	0.316	0.592	0.84
PatchTST	0.940	0.824	0.813	0.657	0.921	0.879	0.741	0.714	0.811	0.911
FiLM	0.907	0.665	0.495	0.315	0.790	0.591	0.412	0.331	0.563	0.832
TimesNet	0.957	0.864	**0.871**	0.644	**0.943**	0.571	0.879	0.792	0.815	0.926
Bi-LSTM	**0.968**	**0.911**	0.864	**0.828**	0.810	0.787	0.789	0.717	0.834	**0.94**

The quantified information of the cropping structure results is given in Table 5. The study area's agricultural cultivation scale encompasses 5.29×10^5 hectares (hm^2), spanning 853,404 parcels. In contrast to the large-scale cultivation observed in corps cities like Shihezi, agriculture in the Weigan River Basin predominantly adheres to a smallholder economy model. The average parcel area is 6202 m^2, featuring a smaller area than the Xinjiang Production and Construction Corps' cropland. This is primarily attributed to the decentralized agricultural operation and smallholder economy prevailing in the county-level area. Regarding the types of crops, the predominant ones in the region are cotton and corn, covering areas of 404,326 hm^2 and 66,480 hm^2, respectively. Specialized crops include peppers (14,340 hm^2) and tomatoes (1871 hm^2), while traditional fruit trees such as jujube, pear, and apricot occupy areas of 47,354 hm^2, 21,332 hm^2, and 4239 hm^2, respectively.

Fruit trees, peppers, and other specialized crops are predominantly situated in the peripheries of towns and cities for ease of daily management. Conversely, cotton and corn are primarily distributed along the two sides of the Weigan River and the Tarim River's middle reaches, facilitating irrigation practices. Cultivated land in the middle reaches of the Tarim River has primarily been reclaimed in previous years, but in recent years, some areas have been abandoned, and there is some fallow land on the edge of the oasis.

The study area primarily encompasses the main urban areas of Shaya, Xinhe, and Kuche counties on the western edge of the Tarim Basin, along with portions of Yuli and Luntai counties situated on the northern edge of the Tarim Basin. The cropping structures within this basin exhibit broad similarities attributed to uniform irrigation methods.

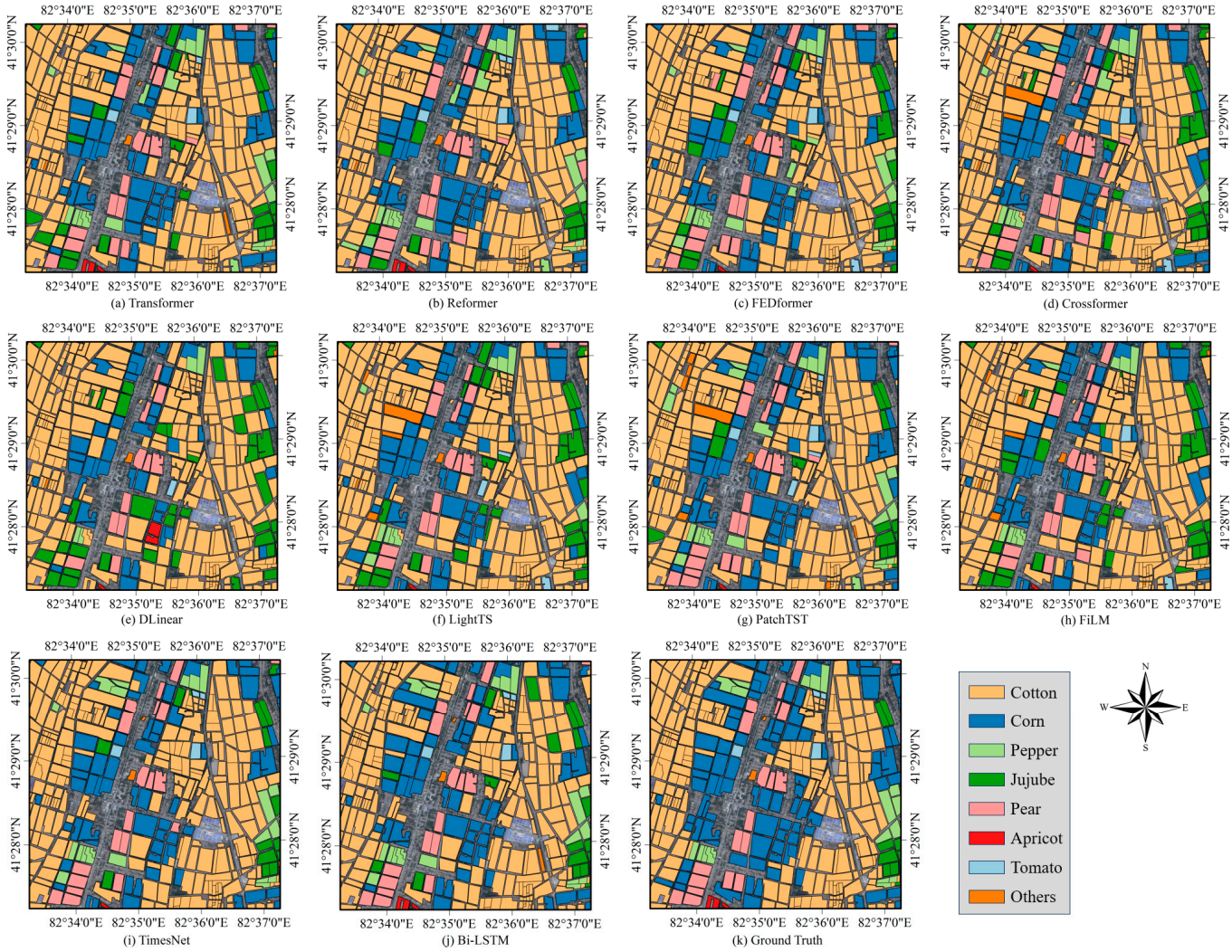

Figure 5. Illustration of parcel-level crop classification results on an test image using different time-series models. (**a**–**j**) Classification results of different models; (**k**) ground truth.

Table 5. Quantified cropping structure in the Weigan River Basin.

Crops	Number of Parcels	Total Area (ha)	Proportion of Parcels	Area Ratio	Average Area (m^2)
Cotton	589,398	404,326	69.04%	76.34%	6860
Corn	157,123	66,480	18.42%	12.55%	4230
Jujube	47,354	21,332	5.55%	4.03%	4504
Pepper	15,297	14,340	1.79%	2.71%	9374
Pear	29,432	15,942	3.45%	3.01%	5418
Apricot	4239	1526	0.50%	0.29%	3600
Tomato	4655	1871	0.55%	0.35%	4021
Others	5866	3826	0.69%	0.72%	6522

Figure 6 is the visualization of crop planting area proportions in the Weigan River Basin, which was divided into two regions by different water utilization coefficients. The first region includes Kuche, Shaya, and Xinhe, featuring a water utilization coefficient of 0.682. The second region includes Luntai and Yuli, featuring a water utilization coefficient of 0.65. The water utilization coefficients were derived from the "Xinjiang Uygur Autonomous Region Agricultural Irrigation-water Quota Indicators". Cotton is the primary crop with significant economic value and dominates the whole planting area. The crop structure

of the region with a water utilization coefficient of 0.682 is relatively homogeneous, with maize as the second major crop constituting 12.78%, and the proportion of cotton, corn, and other major crops reaching nearly 90%. The crop structure of the region with a water utilization coefficient of 0.65 is relatively balanced, with corn, peppers, and jujube trees planted in similar proportions of more than 4%, and the area has a significant ad-vantage in the cultivation of specialty crops.

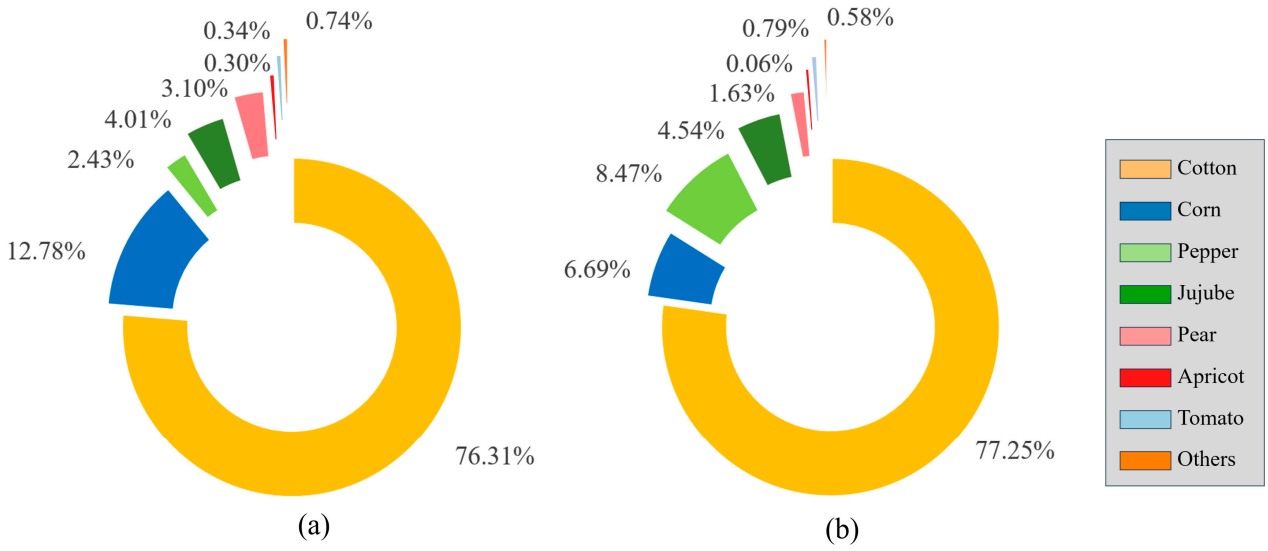

Figure 6. Visualization of crop planting area proportions in the Weigan River Basin. (**a**) Region using a water utilization coefficient of 0.682; (**b**) region using a water utilization coefficient of 0.65.

4.2. Irrigation Demand

According to the "Xinjiang Uygur Autonomous Region Agricultural Irrigation-water Quota Indicators", the Weigan River Basin exhibits an overall water-saving irrigation rate of approximately 78.3%, so a 75% irrigation design guarantee rate (p = 75%) was adopted. The water demand for crop irrigation in the Weigan River Basin can be determined using Equation (7), and the corresponding results are presented in Table 6.

Table 6. The detailed irrigation-water demand in the Weigan River Basin. The water-use coefficient is 0.682 in Kuqa, Shaya, and Xinhe and 0.65 in Luntai and Yuli. The table also provides the irrigation-water demand of major crops under different irrigation methods and gives the upper and lower limits of the irrigation-water demand with coefficients of 0.1 and 0.08, respectively.

Region	Type	Irrigation Method	Cotton	Corn	Pepper	Jujube	Pear	Apricot	Tomato	Others
Kuche Shaya Xinhe	irrigation quota (m^3/ha)	conventional	570	485	480	450	460	455	450	455
		water-saving	295	250	245	320	330	325	225	235
	irrigation-water (10^7 m^3)	conventional	71.65	10.25	1.93	2.28	2.97	0.25	0.23	0.55
		water-saving	133.81	19.06	3.55	5.85	5.36	0.64	0.59	1.02
Luntai Yuli	irrigation quota (m^3/ha)	conventional	615	490	500	680	730	700	480	460
		water-saving	300	240	260	320	340	320	245	225
	irrigation-water (10^7 m^3)	conventional	3.63	0.25	0.33	0.08	0.17	0.04	0.01	0.02
		water-saving	6.39	0.44	0.61	0.14	0.31	0.07	0.01	0.03
Total	the upper limit of irrigation-water demand		29.97×10^8 m^3							
	the average irrigation-water demand		27.24×10^8 m^3							
	the lower limit of irrigation-water demand		25.07×10^8 m^3							

Table 6 reveals that water-saving irrigation methods reduce unnecessary evaporation and seepage, leading to a substantial 50% reduction in the corresponding irrigation-water requirement quota. Nevertheless, given that 78.3% of the arable land is subjected to water-saving irrigation, the water-saving irrigated arable land area is approximately four times larger than that under conventional irrigation. Despite a reduced irrigation quota, the water quantity used in water-saving irrigation for each crop type remains about 1.8 times greater than that used in conventional irrigation. There are substantial variations in irrigation quotas for the same crop among different crops and between different irrigation districts. Coupled with the imbalance in planting structure, these variations result in significant differences in the water requirements of different crops. Major crops like cotton and corn have substantial irrigation quotas, and the significant proportion of cotton area results in cotton and corn collectively accounting for 90.11% of the irrigation-water demand. In contrast, for the other crops, their limited planting area causes their irrigation-water demand to constitute 9.89% of the total. Although their proportion of irrigation-water demand is not high, fruit trees such as jujube, pear, and apricot have large irrigation quotas.

In 2020, the irrigation-water demand amounted to 27.24×10^8 m^3. However, considering the intricate meteorological and hydrological conditions and to ensure the scientific calculation of crop water demand, coefficients of 0.1 (upper limit) and 0.08 (lower limit) were applied to determine the amount of irrigation water in the study area. The required irrigation is relatively reduced in years of abundant water characterized by high precipitation. This is calculated based on the lower limit of the irrigation-water demand, resulting in a required amount of about 25.07×10^8 m^3. Artificial irrigation must be increased in dry years, marked by intense evaporation. This is then calculated based on the upper limit of irrigation-water demand, resulting in a required amount of about 29.97×10^8 m^3.

4.3. Irrigation Supply

The surface runoff W_r and the non-repeatable underground water resource W_u values are derived from publications such as the *2020 Water Resources Bulletin, Xinjiang Statistical Yearbook, Aksu Statistical Yearbook*, etc., where surface runoff statistics exhibit considerable variation. Within the Tarim system, the Weigan River system is the most minor yet remarkably stable water system, exhibiting minimal inter-annual variation in water quantity. It primarily comprises the Weigan, Kuche, Heizi, Muzhaerte, and Kalasu Rivers, as well as numerous small tributaries from this river. The runoff recharge of the Weigan River system, considering surface runoff as a weight, consists of 51.7% glacial meltwater, 23.3% groundwater, and 25.0% rain and snow.

Using hydrological data, we can develop an enclosed system for balancing water supply and demand. Specifically, the Heizi reservoir hydrological station in the upper reaches of the Weigan River, Langan hydrological station in the upper reaches of the Kuche River, and Aral hydrological station in the middle reaches of the Tarim River serve as monitoring stations for the inlet flow; the Yingbazha hydrological station in the middle and lower reaches of the Tarim River serves as the monitoring station for the outlet flow. In 2020, the surface runoff of the Weigan River basin was 44.15×10^8 m^3, and the groundwater volume was 4.15×10^8 m^3. Precipitation in the Weigan River basin is relatively low, measuring only 156.7 mm in 2020, per meteorological station data. However, in the arid region of the Weigan River, precipitation remains a crucial form of water resource replenishment. Precipitation recharge in this basin amounts to 22.27×10^8 m^3 [40]. Therefore, the total incoming water of the Weigan River Basin is 70.57×10^8 m^3, with surface water resources constituting approximately 94.12% of the total.

Considering various types of water consumption and utilizing the per capita domestic water consumption quota alongside population data, domestic water consumption W_l of the Weigan River Basin totals 4.7×10^8 m^3. Based on the industrial GDP output value and industrial water consumption totaling CNY 10,000 of the GDP, industrial water consumption W_i is estimated at 0.35×10^8 m^3. According to the water consumption quota

for animal husbandry and the basin's livestock population, the water consumption for animal husbandry is 0.07×10^8 m^3.

Ecological water consumption comprises evapotranspiration, channel balance, and vegetation-water consumption. Initially, lakes and reservoirs' evapotranspiration, determined by Penman's formula [41] based on the watershed area, is 2.21×10^8 m^3. River balance primarily encompasses water resources consumed in natural river channels to maintain ecosystem stability and water consumed by the ecological use of channel seepage water by bank protection forests in artificial irrigation canals. Empirical coefficients suggest that 30% of surface runoff is typically consumed for river balance in arid-zone watersheds. Consequently, it can be inferred that river balance consumes a minimum of 13.24×10^8 m^3 of water. Due to the continuous decrease in cultivated land area in the middle reaches of the Tarim River over the past five years, ecological conditions have improved. According to the relevant literature, the water consumption of natural vegetation in the Weigan River Basin is estimated to be 25.57×10^8 m^3 [42]. In 2020, the total water consumption of the Weigan River Basin, excluding irrigation-water consumption, amounts to about 46.17×10^8 m^3. According to the water balance approach, prioritizing ecological water consumption, the irrigation-water supply should be 24.4×10^8 m^3. A graphical representation for each term of the water balance, as given by Equation (7), is given in Figure 7.

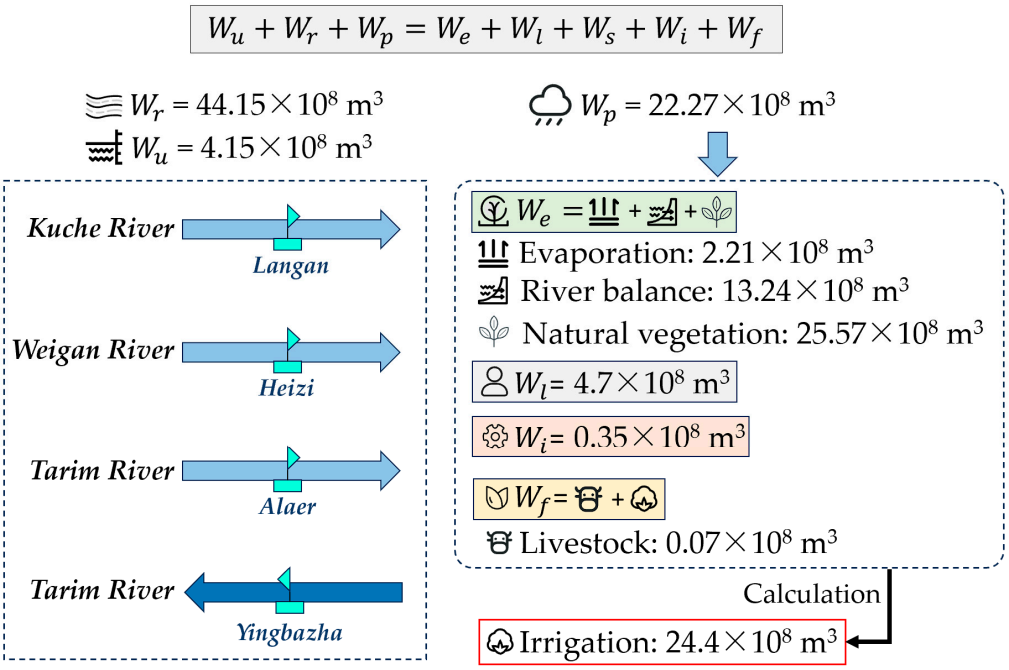

Figure 7. Visualization of the irrigation supply based on a water balance approach.

5. Discussion

5.1. Differences in Irrigation-Water Demand Estimation Using Pixel-Level and Parcel-Level Mapping in Arid Regions

The downstream area of the Weigan River Basin, particularly the large farmland parcels, experiences severe soil salinization. The land must be irrigated to wash away the salts. However, even with this measure, many cultivated lands remain of low quality, resulting in patchy and fragmented crop growth. In such circumstances, the crop area obtained through pixel-level classification is smaller than the actual sown area, leading to an underestimation of the calculated irrigation-water requirements. In contrast, parcel-level crop distribution mapping is not influenced by the crop growth conditions within the farmland parcels and is particularly suitable for the prevalent situation in the study area where the actual crop growth area is less than the sown area.

Table 7 provides a comprehensive comparison of irrigation-water demand estimation based on pixel-level and parcel-level cropping structures for various crops in the Weigan River Basin, highlighting both the percentage of parcel numbers with different crop pixel coverages and the total area and water demand for each crop. The parcel-level mapping consistently shows higher total areas for each crop type compared to the pixel-level mapping. Overall, the total irrigation-water demand across all crops is underestimated by 14.38 $\times$ 10^7 m^3 when using pixel-level mapping. This discrepancy is particularly pronounced in the case of cotton, which dominates the region's agricultural landscape. Parcel-level mapping estimates 404,326 hectares of cotton, compared to 379,947 hectares from pixel-level mapping, leading to an irrigation-water demand difference of 12.99 $\times$ 10^7 m^3. This underestimation in cotton accounts for the vast majority of the total discrepancy between the two mapping methods, as cotton occupies over 75% of the cultivated area in the study region. Another key factor driving this significant difference is the location and condition of cotton fields. Cotton is often grown on the outer fringes of the basin, where severe soil salinization degrades land quality, making these parcels more prone to patchy growth. In contrast, higher-value crops such as pepper and jujube, typically cultivated on smaller, higher-quality parcels by farmers, experience fewer discrepancies between mapping methods.

Table 7. The detailed differences in irrigation-water demand estimation based on pixel-level and parcel-level cropping structures in the study area.

Crop Type		Cotton	Corn	Pepper	Jujube	Pear	Apricot	Tomato	Others
The percentage of parcel numbers with different crop pixel coverage	<0.5	0.42%	0.05%	0.00%	0.12%	0.01%	0.05%	0.00%	0.39%
	0.5–0.6	0.36%	0.07%	0.00%	0.05%	0.03%	0.05%	0.00%	0.17%
	0.6–0.7	0.64%	0.17%	0.02%	0.06%	0.10%	0.23%	0.32%	0.27%
	0.7–0.8	1.12%	0.36%	0.09%	0.15%	0.22%	0.00%	0.25%	0.44%
	0.8–0.9	2.17%	1.15%	0.24%	0.18%	0.44%	0.32%	1.16%	1.03%
	0.9–0.95	4.28%	3.95%	0.67%	0.77%	1.44%	0.96%	2.18%	2.31%
	>0.95	91.01%	94.25%	98.98%	98.67%	97.76%	98.39%	96.10%	95.37%
Total area (ha)	Parcel-level	404,326	66,480	21,332	14,340	15,942	1526	1871	3826
	Pixel-level	379,947	64,457	20,995	14,010	15,778	1506	1825	3702
Irrigation-water demand estimation (10^7 m^3)	Parcel-level	215.48	30	6.42	8.35	8.81	1	0.84	1.62
	Pixel-level	202.49	29.09	6.32	8.16	8.72	0.99	0.82	1.57

Figure 8 takes the eastern downstream area of the Weigan River Basin as an example to demonstrate the differences in irrigation-water requirements calculated using pixel-level and plot-level crop distribution mapping. Figure 8a–d show images of the area from June to September. The reclaimed farmland is surrounded by saline–alkaline land. It can be observed that the crop growth in many farmland parcels within the study area is poor (as indicated by the red arrows), appearing patchy and fragmented. Figure 8f,g present the distribution of farmland parcel irrigation-water requirements calculated based on pixel-level and parcel-level crop mapping, respectively. Figure 8h visualizes the differences between the two, with farmland parcel colors representing the ratio of irrigation-water requirements obtained from pixel-level mapping to those obtained from parcel-level mapping. The actual crop growth area obtained through pixel-level crop mapping is lower than the actual farmland parcel area used to determine irrigation-water requirements. According to Equation (7), the calculated irrigation-water requirements are also underestimated. The differences are even more pronounced in large mechanized farmland parcels. Firstly, they experience more severe salinization. Additionally, compared to smallholder farming areas, farmers often manage their farmland parcels more meticulously, leading to higher crop survival rates. This solution is particularly suitable for saline–alkaline land in Xinjiang and can be extended to areas where cultivated land quality is insufficient or where the sown area is smaller than the growth area.

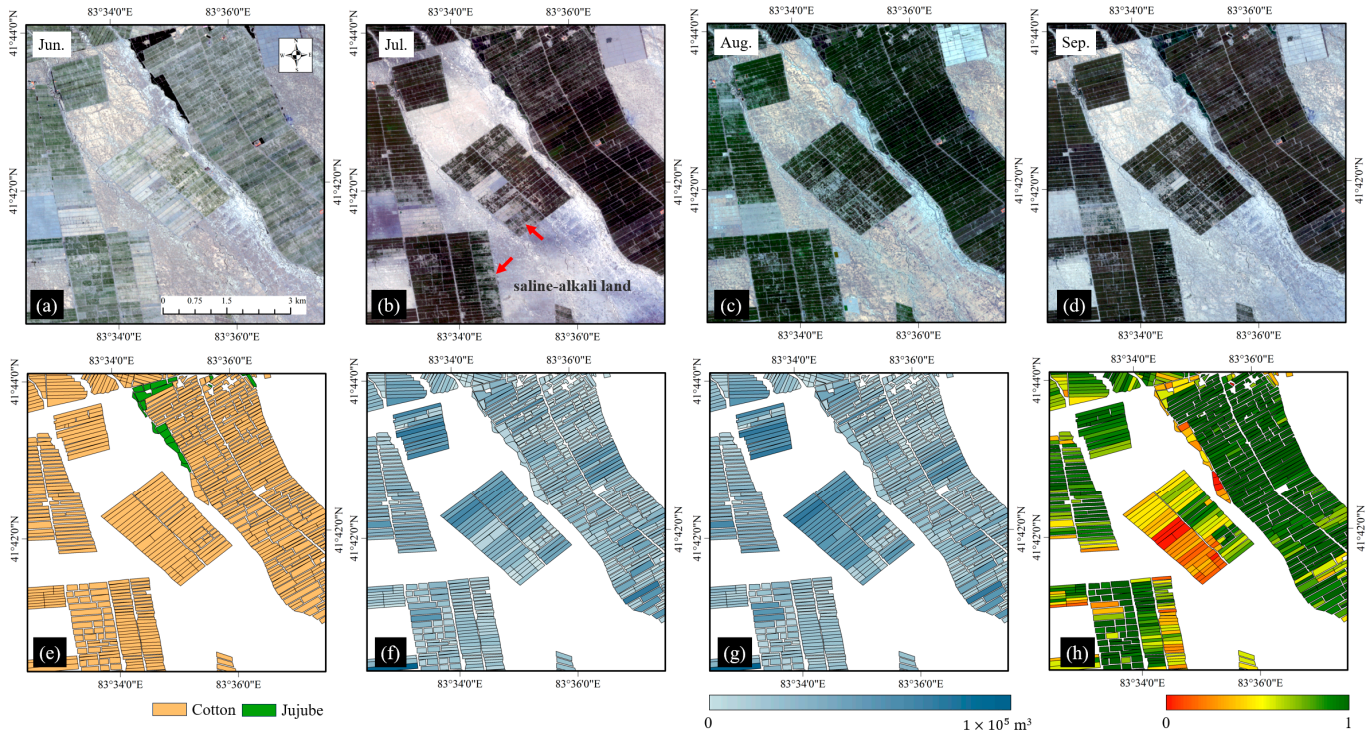

Figure 8. An example of a study area estimating the irrigation-water demand through pixel- and parcel-level crop structure. (**a**–**d**) Sentinel-2 images of the region from Jun. to Sep.; (**e**) parcel-aggregated crop structure; (**f**) distribution of irrigation-water demand based on pixel-level cropping structure; (**g**) distribution of irrigation-water demand based on parcel-aggregated cropping structure; (**h**) visualization of differences between (**f**,**g**).

5.2. Limitations of the Study

This strategy has high requirements for cropping structure accuracy. The accuracy of farmland parcel extraction directly affects the precision of calculated irrigation-water requirements. This is why we still adopt a semi-automated approach for farmland parcel extraction. During the pre-extraction of farmland parcels, we have a higher tolerance for oversegmentation, as it does not directly impact the calculation of irrigation-water requirements. However, undersegmentation of farmland parcels has a greater impact on the calculation error of irrigation-water requirements. Due to the error propagation effect, this not only affects the subsequent classification of crop types based on the temporal mean spectral values within the farmland parcels but also directly impacts the accuracy of calculated irrigation-water requirements. The issue of undersegmentation is mainly caused by weak visual features and strong heterogeneity at the edges of farmland parcels. The identification of farmland parcels still heavily relies on expert knowledge and cannot be simply explained as a visual problem. Additionally, although there are strict irrigation quota restrictions in arid regions, dynamic adjustments still occur during actual implementation. Particularly in smallholder farming areas, farmer management is random. Furthermore, the surface water system in the study area of this research is relatively enclosed. For study areas with more complex water systems, the application still requires optimization.

5.3. Suggestions Based on Irrigation Supply and Demand Analysis

The agricultural water consumption in the Weigan River Basin for 2020 is estimated at 24.4×10^8 m^3. This value falls short of the lower limit of 25.07×10^8 m^3 for irrigation-water demand in a year of abundant water in the region. Nevertheless, agricultural authorities compensate for the irrigation-water gap in practical production by displacing vegetation-water consumption. In recent years, the gradual farmland optimization has somewhat mitigated the water usage conflict between arable land and natural forests and grasses. It

has also enabled a partial supplementation of ecological water use. However, historical over-exploitation of land has left the region's arable land scale significantly exceeding the carrying capacity of water resources, posing a heightened threat to the protection of groundwater resources.

In analyzing the contradiction between water resource supply and demand, adjustments to agriculture in the basin are recommended as follows:

(1) Convert farmland. The region should undertake efforts to convert farmland into forests and grasslands in the southern part of the Weigan River Basin and the middle reaches of the Tarim River to uphold the ecological security of the river.
(2) Adjust the agricultural planting structure. The water demand per unit area is excessively high since nearly 80% of the region's crops consist of high-water-consuming varieties such as cotton and fruit trees. For instance, cotton's water consumption reaches 79.6%. A 10% reduction in its planting area could save 2.1×10^8 m^3 of irrigation water. Low-water-consuming crops like tomatoes can be cultivated in areas distant from the river and with weak soil fertility, reducing transpiration losses.
(3) Enhance the water-saving irrigation rate. Situated in the middle reaches of the Tarim River, the Weigan River Basin has relatively straightforward glacier recharge and surface water extraction. Though commendable, the 78.3% water-saving irrigation rate lags behind the 87% rate in the Northern Xinjiang Irrigation Area. There is significant potential for improvement. Therefore, agricultural irrigation methods should be optimized to minimize unnecessary seepage and evaporation.

6. Conclusions

Accurate estimation of irrigation-water demand in arid regions is crucial for sustainable agricultural water resource management. However, traditional pixel-level mapping often underestimates irrigation-water demand in regions like the Weigan River Basin due to poor crop growth caused by land salinization. To address this issue, this study adopts a parcel-aggregated cropping structure mapping method, providing a more accurate representation of agricultural land use that aligns better with the implementation of irrigation plans at the field level. By employing deep learning models—the RCF for parcel delineation and the Bi-LSTM for time-series classification—this study extracts precise cropping structures within the Weigan River Basin, Xinjiang, China. Subsequently, the water balance approach was used to estimate the region's irrigation-water consumption. Finally, we analyzed the disparity between irrigation supply and demand and recommended balancing agricultural and ecological benefits. The conclusions were as follows:

(1) In 2020, the cultivated area of the Weigan River Basin was 5.29×10^5 ha, encompassing a total of 853,404 parcels, with an average parcel size of 6202 m^2. The primary crops include cotton and corn, constituting about 76.34% of the arable land area.
(2) Based on the parcel-level cropping structure, the irrigation-water demand in 2020 was 27.24×10^8 m^3, which is 1.44×10^8 m^3 higher than the demand estimated using the pixel-level cropping structure. Using the upper coefficient of 0.1 and the lower limit coefficient of 0.08, the irrigation-water demand for this year was expected to range between 25.07×10^8 m^3 and 29.97×10^8 m^3. Following a water balance approach, deducting the remaining water consumption, the actual irrigation supply was estimated at 24.4×10^8 m3, resulting in a shortfall of 0.64×10^8 m^3 from the lower limit of irrigation demand.
(3) The displacement of ecological water by irrigation water in the Weigan River Basin has intensified ecological instability and depleted the ecological health of the lower reaches of the Tarim River. It is recommended that farmland be converted into forests and grasslands, preserving the ecological safety of the river. Furthermore, the approach to water resource allocation should shift from "determining water policies based on farmland conditions" to "determining farmland structures based on the current status of water resources".

Author Contributions: Conceptualization, S.L., H.W. and C.W.; methodology, S.L., H.W., J.L. and Z.S.; validation, C.Z. (Chenghu Zhou), T.V.d.V. and P.D.M.; formal analysis, C.W. and S.L.; investigation, L.B.; resources, L.B.; data curation, W.K. and C.Z. (Chi Zhang); writing—original draft preparation, L.B.; writing—review and editing, L.B., H.W., Z.S. and T.V.d.V.; visualization, H.W.; supervision, C.Z. (Chenghu Zhou), T.V.d.V. and P.D.M.; project administration, Z.S.; funding acquisition, J.L. and Z.S. All authors have read and agreed to the published version of the manuscript.

Funding: This research was funded by the Third Integrated Scientific Expedition Project in Xinjiang (2021xjkk1403), the National Natural Sciences Foundation of China (U2003201), the Key Research and Development Program of Xinjiang Uygur Autonomous Region (2022B03001-3), the Tianshan Talent-Science and Technology Innovation Team (2022TSYCTD0006) and the Chinese Academy of Sciences President's International Fellowship Initiative (2024PVB0064).

Data Availability Statement: The data presented in this study are available on request from the corresponding author.

Acknowledgments: We sincerely appreciate the assistance provided by Yubo Ma.

Conflicts of Interest: The authors declare no conflicts of interest.

References

1. Wu, K.; Ye, X.; Qi, Z.; Zhang, H. Impacts of land use/land cover change and socioeconomic development on regional ecosystem services: The case of fast-growing Hangzhou metropolitan area, China. *Cities* **2013**, *31*, 276–284. [CrossRef]
2. Hao, P.; Zhan, Y.; Wang, L.; Niu, Z.; Shakir, M. Feature Selection of Time Series MODIS Data for Early Crop Classification Using Random Forest: A Case Study in Kansas, USA. *Remote Sens.* **2015**, *7*, 5347–5369. [CrossRef]
3. Doraiswamy, P. Crop condition and yield simulations using Landsat and MODIS. *Remote Sens. Environ.* **2004**, *92*, 548–559. [CrossRef]
4. Wang, N.; Hao, J.; Zhang, L.; Duan, W.; Shi, Y.; Zhang, J.; Wusimanjiang, P. Basic Farmland Protection System in China: Changes, Conflicts and Prospects. *Agronomy* **2023**, *13*, 651. [CrossRef]
5. Liang, X.; Jin, X.; Han, B.; Sun, R.; Xu, W.; Li, H.; He, J.; Li, J. China's food security situation and key questions in the new era: A perspective of farmland protection. *J. Geogr. Sci* **2022**, *32*, 1001–1019. [CrossRef]
6. Zhuo, W.; Huang, J.; Gao, X.; Ma, H.; Huang, H.; Su, W.; Meng, J.; Li, Y.; Chen, H.; Yin, D. Prediction of Winter Wheat Maturity Dates through Assimilating Remotely Sensed Leaf Area Index into Crop Growth Model. *Remote Sens.* **2020**, *12*, 2896. [CrossRef]
7. Jalilvand, E.; Tajrishy, M.; Ghazi Zadeh Hashemi, S.A.; Brocca, L. Quantification of irrigation water using remote sensing of soil moisture in a semi-arid region. *Remote Sens. Environ.* **2019**, *231*, 111226. [CrossRef]
8. Kanda, E.K.; Lutta, V.O. The status and challenges of a modern irrigation system in Kenya: A systematic review. *Irrig. Drain.* **2022**, *71*, 27–38. [CrossRef]
9. Mishra, S.; Issac, A.M.; Singh, R.; Raju, P.V.; Vala, V.R. Mapping of intra-season dynamics in the cropping pattern using remote sensing for irrigation management. *Geocarto Int.* **2022**, *37*, 4994–5016. [CrossRef]
10. Han, X.; Wei, Z.; Zhang, B.; Han, C.; Song, J. Effects of Crop Planting Structure Adjustment on Water Use Efficiency in the Irrigation Area of Hei River Basin. *Water* **2018**, *10*, 1305. [CrossRef]
11. Ma, Y.; Xue, J.; Feng, X.; Zhao, J.; Tang, J.; Sun, H.; Chang, J.; Yan, L. Crop water productivity assessment and planting structure optimization in typical arid irrigation district using dynamic Bayesian network. *Sci. Rep.* **2024**, *14*, 17695. [CrossRef] [PubMed]
12. Zhang, J.; Guan, K.; Zhou, W.; Jiang, C.; Peng, B.; Pan, M.; Grant, R.F.; Franz, T.E.; Suyker, A.; Yang, Y.; et al. Combining Remotely Sensed Evapotranspiration and an Agroecosystem Model to Estimate Center-Pivot Irrigation Water Use at High Spatio-Temporal Resolution. *Water Resour. Res.* **2023**, *59*, e2022WR032967. [CrossRef]
13. Xu, H.; Duan, H.; Li, Q.; Han, C. Identification of Actual Irrigated Areas in Tropical Regions Based on Remote Sensing Evapotranspiration. *Atmosphere* **2024**, *15*, 492. [CrossRef]
14. Wei, S.; Xu, T.; Niu, G.-Y.; Zeng, R. Estimating Irrigation Water Consumption Using Machine Learning and Remote Sensing Data in Kansas High Plains. *Remote Sens.* **2022**, *14*, 3004. [CrossRef]
15. Reyes-González, A.; Kjaersgaard, J.; Trooien, T.; Hay, C.; Ahiablame, L. Estimation of Crop Evapotranspiration Using Satellite Remote Sensing-Based Vegetation Index. *Adv. Meteorol.* **2018**, *2018*, 4525021. [CrossRef]
16. Sainath, T.N.; Kingsbury, B.; Saon, G.; Soltau, H.; Mohamed, A.R.; Dahl, G.; Ramabhadran, B. Deep Convolutional Neural Networks for Large-scale Speech Tasks. *Neural Netw.* **2015**, *64*, 39–48. [CrossRef]
17. Chen, L.C.; Papandreou, G.; Kokkinos, I.; Murphy, K.; Yuille, A.L. DeepLab: Semantic Image Segmentation with Deep Convolutional Nets, Atrous Convolution, and Fully Connected CRFs. *IEEE Trans. Pattern Anal. Mach. Intell.* **2018**, *40*, 834–848. [CrossRef]
18. Hochreiter, S.; Schmidhuber, J. Long short-term memory. *Neural Comput.* **1997**, *9*, 1735–1780. [CrossRef]
19. Wang, H.; Shen, Z.; Zhang, Z.; Xu, Z.; Li, S.; Jiao, S.; Lei, Y. Improvement of Region-Merging Image Segmentation Accuracy Using Multiple Merging Criteria. *Remote Sens.* **2021**, *13*, 2782. [CrossRef]

20. Hossain, M.D.; Chen, D. Segmentation for Object-Based Image Analysis (OBIA): A review of algorithms and challenges from remote sensing perspective. *ISPRS J. Photogramm. Remote Sens.* **2019**, *150*, 115–134. [CrossRef]
21. Zhao, F.; Xiong, L.Y.; Wang, C.; Wang, H.R.; Wei, H.; Tang, G.A. Terraces mapping by using deep learning approach from remote sensing images and digital elevation models. *Trans. GIS* **2021**, *25*, 2438–2454. [CrossRef]
22. Dai, W.; Na, J.M.; Huang, N.; Hu, G.H.; Yang, X.; Tang, G.A.; Xiong, L.Y.; Li, F.Y. Integrated edge detection and terrain analysis for agricultural terrace delineation from remote sensing images. *Int. J. Geogr. Inf. Sci.* **2020**, *34*, 484–503. [CrossRef]
23. Liu, T.; Shao, F.; Zhang, Z.; Li, T. Fluorine-Rich Shallow Groundwater in Weigan River Basin (Xinjiang): Enrichment Factors and Spatial Distribution. *Water* **2023**, *15*, 926. [CrossRef]
24. Wu, H.; Xu, M.; Peng, Z.; Chen, X. Quantifying the potential impacts of meltwater on cotton yields in the Tarim River Basin, Central Asia. *Agric. Water Manag.* **2022**, *269*, 107639. [CrossRef]
25. Barak, P. Smoothing and Differentiation by an Adaptive-Degree Polynomial Filter. *Anal. Chem.* **1995**, *67*, 2758–2762. [CrossRef]
26. Jing, R.; Liu, S.; Gong, Z.N.; Wang, Z.H.; Guan, H.L.; Gautam, A.; Zhao, W.J. Object-based change detection for VHR remote sensing images based on a Trisiamese-LSTM. *Int. J. Remote Sens.* **2020**, *41*, 6209–6231. [CrossRef]
27. Cui, W.; Zhang, D.Y.; He, X.; Yao, M.; Wang, Z.W.; Hao, Y.J.; Li, J.; Wu, W.J.; Cui, W.Q.; Huang, J.J. Multi-Scale Remote Sensing Semantic Analysis Based on a Global Perspective. *ISPRS Int. J. Geo-Inf.* **2019**, *8*, 417. [CrossRef]
28. Cui, W.; Wang, F.; He, X.; Zhang, D.Y.; Xu, X.X.; Yao, M.; Wang, Z.W.; Huang, J.J. Multi-Scale Semantic Segmentation and Spatial Relationship Recognition of Remote Sensing Images Based on an Attention Model. *Remote Sens.* **2019**, *11*, 1044. [CrossRef]
29. Li, L.; Doroslovački, M.; Loew, M.H. Approximating the Gradient of Cross-Entropy Loss Function. *IEEE Access* **2020**, *8*, 111626–111635. [CrossRef]
30. Jing, Y. Application fo water-balance principle to analysis and calculation for water-consumption of river basin. *Northwest Water Resour. Water Eng.* **2003**, *14*, 30–32. [CrossRef]
31. Vaswani, A.; Shazeer, N.; Parmar, N.; Uszkoreit, J.; Jones, L.; Gomez, A.N.; Kaiser, L.; Polosukhin, I. Attention Is All You Need. *arXiv* **2017**, arXiv:1706.03762. [CrossRef]
32. Kitaev, N.; Kaiser, Ł.; Levskaya, A. Reformer: The Efficient Transformer. *arXiv* **2020**, arXiv:2001.04451. [CrossRef]
33. Zhou, T.; Ma, Z.; Wen, Q.; Wang, X.; Sun, L.; Jin, R. FEDformer: Frequency Enhanced Decomposed Transformer for Long-term Series Forecasting. *arXiv* **2022**, arXiv:2201.12740. [CrossRef]
34. Wang, W.; Yao, L.; Chen, L.; Lin, B.; Cai, D.; He, X.; Liu, W. CrossFormer: A Versatile Vision Transformer Hinging on Cross-scale Attention. *arXiv* **2021**, arXiv:2108.00154. [CrossRef] [PubMed]
35. Zeng, A.; Chen, M.; Zhang, L.; Xu, Q. Are Transformers Effective for Time Series Forecasting? *arXiv* **2022**, arXiv:2205.13504. [CrossRef]
36. Zhang, T.; Zhang, Y.; Cao, W.; Bian, J.; Yi, X.; Zheng, S.; Li, J. Less Is More: Fast Multivariate Time Series Forecasting with Light Sampling-oriented MLP Structures. *arXiv* **2022**, arXiv:2207.01186. [CrossRef]
37. Nie, Y.; Nguyen, N.H.; Sinthong, P.; Kalagnanam, J. A Time Series is Worth 64 Words: Long-term Forecasting with Transformers. *arXiv* **2022**, arXiv:2211.14730. [CrossRef]
38. Zhou, T.; Ma, Z.; Wang, X.; Wen, Q.; Sun, L.; Yao, T.; Yin, W.; Jin, R. FiLM: Frequency improved Legendre Memory Model for Long-term Time Series Forecasting. *arXiv* **2022**, arXiv:2205.08897. [CrossRef]
39. Wu, H.; Hu, T.; Liu, Y.; Zhou, H.; Wang, J.; Long, M. TimesNet: Temporal 2D-Variation Modeling for General Time Series Analysis. *arXiv* **2022**, arXiv:2210.02186. [CrossRef]
40. Wang, C.; Du, H.; Zhang, X.; Wang, F.; Zhang, L.; Li, X. Analysis of relative carrying capacity of resources in Tarim River Basin in Xinjiang. *Acta Ecol. Sin.* **2015**, *35*, 2880–2893. [CrossRef]
41. Penman, H.L. Natural Evaporation from Open Water, Bare Soil and Grass. *Proc. R. Soc. Lond. Ser. A-Math. Phys. Sci.* **1948**, *193*, 120–145. [CrossRef]
42. Kang, X.; Wang, X. Assessment of ecological risk of Weigan-Kuqa River Delta Oasis in Xinjiang based on landscape pattern. *J. Northwest A F University. Nat. Sci. Ed.* **2017**, *45*, 139–146,156. [CrossRef]

Disclaimer/Publisher's Note: The statements, opinions and data contained in all publications are solely those of the individual author(s) and contributor(s) and not of MDPI and/or the editor(s). MDPI and/or the editor(s) disclaim responsibility for any injury to people or property resulting from any ideas, methods, instructions or products referred to in the content.